Journal of Luminescence 286 (2025) 121333

Contents lists available at ScienceDirect

Journal of Luminescence

journal homepage: www.elsevier.com/locate/jlumin

Full Length Article

Pr^{3+}-doped $RbCaF_3$: a new X-ray-induced UVC persistent phosphor

Nadiia Rebrova [a,*], Andriy Pushak [b], Alexander Grippa [c], Vitalii Boiko [a,d], Patrycja Zdeb-Stańczykowska [a], Anatoliy Voloshinovskii [b], Przemysław J. Dereń [a]

[a] Institute of Low Temperature and Structure Research, Polish Academy of Science, ul. Okólna 2, 50-422, Wrocław, Poland
[b] Ivan Franko National University of Lviv, 8 Kyryla i Mefodiya St, 79005, Lviv, Ukraine
[c] Institute for Scintillation Materials, National Academy of Sciences of Ukraine, Nauky Avenue, 60, 61001, Kharkiv, Ukraine
[d] Department of Physics of Biological Systems, Institute of Physics, National Academy of Sciences of Ukraine, Prospekt Nauky, 46, UA-03028, Kyiv, Ukraine

ARTICLE INFO

Keywords:
Perovskite
Rare earth
Optical materials
Optical properties
Persistent luminescence

ABSTRACT

The development of persistent ultraviolet-emitting phosphors is advancing rapidly because of their promising applications in alternative cancer treatments. In this work, we developed a novel Pr^{3+}-doped $RbCaF_3$ phosphor exhibiting intense long-persistent luminescence in the 220–340 nm range, sustained for more than an hour after just 15 min of X-ray irradiation. The 5d-4f luminescence of Pr^{3+} ions is primarily excited by electron-hole pairs generated during X-ray absorption, as well as by electrons released from traps. The emission and excitation properties of $RbCaF_3$:Pr^{3+} crystallites were further investigated using synchrotron radiation, revealing the simultaneous occurrence of intra-configurational $4f^2 \rightarrow 4f^2$ and inter-configurational $4f5d \rightarrow 4f^2$ radiative transitions upon 4f5d state excitation. This work highlights the potential of Pr^{3+}-doped $RbCaF_3$ phosphor for innovative applications in ultraviolet photonics and cancer therapy.

1. Introduction

One of humanity's greatest challenges is cancer, which according to the World Health Organization, is the second leading cause of death worldwide, with the number of cancer patients continuing to rise each year [1]. Radiation therapy remains a common clinical method for treating inoperable malignant tumors. Although this method is highly effective at killing tumor cells, it also significantly harms healthy cells, resulting in an additional burden on the body. Thus, there is a demand for developing new treatment methods or modifying existing ones to maximize therapeutic benefits while effectively safeguarding the surrounding non-cancerous tissues from damage. An alternative approach to radiation therapy combines traditional X-rays with phosphors that generate UVC radiation (100–280 nm). UVC radiation is particularly effective at being absorbed by nucleic acids in cells, breaking DNA bonds and causing the formation of pyrimidine dimers, which lead to the cessation of transcription and ultimately result in cell death. UVC radiation penetrates tissues only a few micrometers deep, which limits its use against deep tumors [2–4]. To overcome this, nanoparticles placed near tumor cells can absorb penetrating X-rays and convert them into UVC photons. In this way, nanoparticles exert a cytotoxic effect by generating localized UVC light inside the tumor [5–7]. This approach may significantly reduce the dose of X-ray radiation and promote local destruction of cancer cells while increasing the survival of healthy tissues. From the perspective of reducing the radiation dose, special attention is given to compounds that exhibit long-lasting afterglow emission following removal of the X-ray excitation source.

Depending on the host compound and excitation source, the afterglow can persist for periods ranging from a few seconds to several days. Excitation sources may include ionizing radiation, X-rays, ultraviolet light, and, in some cases, visible light. The phenomenon of afterglow has a history spanning thousands of years and was first described in ancient Chinese literature [8]. Over this long period, interest in afterglow has fluctuated. However, the discovery of the material $SrAl_2O_4$:Eu^{2+},Dy^{3+} in 1996 marked the beginning of a new era in afterglow research [9]. The afterglow phenomenon has been referred to as "persistent luminescence", and inorganic materials exhibiting this "persistent luminescence" have become known as "persistent phosphors" [10]. Persistent phosphors involve two types of centers: trap centers and emission centers. Traps can include lattice defects such as oxygen vacancies, F centers, antisite defects, and various impurities [11–13]. Emission centers can include transition metal ions (e.g., Ni^{2+}, Cr^{3+}, Mn^{2+}) with d→d transitions, main group or post-transition metal ions (e.g., Bi^{3+}, Pb^{2+}) with p→s transitions, and lanthanide ions (e.g., Er^{3+}, Eu^{2+}, Ce^{3+}, Nd^{3+}) with

* Corresponding author.
E-mail address: n.rebrova@intibs.pl (N. Rebrova).

https://doi.org/10.1016/j.jlumin.2025.121333
Received 25 March 2025; Received in revised form 12 May 2025; Accepted 31 May 2025
Available online 1 June 2025
0022-2313/© 2025 The Authors. Published by Elsevier B.V. This is an open access article under the CC BY license (http://creativecommons.org/licenses/by/4.0/).

5d→4f or 4f→4f [14–18]. Typically, traps do not emit radiation, but instead store excitation energy for some time, gradually releasing it to emission centers through thermal or other forms of physical activation. The traps primarily determine the intensity and duration of luminescence, while the emission wavelength of a persistent phosphor depends on the luminescent center.

Praseodymium ion (Pr^{3+}) is considered an ideal activator for persistent luminescence in the UVC range. The literature describes matrices doped with Pr^{3+} that exhibit persistent luminescence in the UV range, including phosphates (e.g., YPO_4:Pr^{3+}), fluorides (e.g., Cs_2NaYF_6:Pr^{3+}), germanates (e.g., Li_2CaGeO_4:Pr^{3+}) and silicates (e.g., $LiYSiO_4$:Pr^{3+}) [19–23]. Thus, Pr^{3+} was selected as the activator for this work. ABF_3-type perovskites are promising candidates for persistent luminescence applications due to their structural stability, non-hygroscopic nature, and presence of traps [24,25]. In our previous work, under 444 nm laser excitation, the $RbCaF_3$:Pr^{3+} crystallites exhibited an upconversion band from 230 to 315 nm, demonstrating the potential of these materials for persistent luminescence in the UVC range [26]. However, the X-ray luminescence of $RbCaF_3$:Pr^{3+}, as well as UV luminescence, has not yet been described. This work presents the synthesis and luminescence properties of a new ultraviolet long-persistent phosphor, $RbCaF_3$:Pr^{3+}, under X-ray and synchrotron excitation.

1.1. Experiments

1.1.1. Materials and synthesis

Undoped $RbCaF_3$ and $RbCaF_3$:1 %Pr^{3+}crystallites were synthesized via the solid state method using RbF (99.1 %), CaF_2 (99.99 %), and PrF_3 (99.9 %) as starting materials. No charge compensation was applied. The fluorides were weighed in stoichiometric proportions, ground in an agate mortar for 10 min and then heated to 850 °C and annealed for 8 h in a reducing atmosphere (N_2/H_2). It is worth noting that after two weeks of exposure to 22 °C and 40 ± 2 % relative humidity, $RbCaF_3$:Pr^{3+} showed no measurable weight gain, indicating excellent resistance to moisture absorption.

1.1.2. Sample characterization

The crystal structure was analyzed using powder X-ray diffraction (XRPD) with an X'Pert PRO X-ray diffractometer (CuKα, λ = 1.54056 Å). Morphology was examined by FE-SEM using an FEI Nova NanoSEM 230, with imaging performed at 5.0 kV in slow beam mode. Excitation and emission spectra were recorded at SUPERLUMI (DESY, Germany) using a 2-m McPherson monochromator and a Hamamatsu R6836 photomultiplier. The excitation spectrum was corrected for the incident photon flux using a sodium salicylate reference sample, while the emission spectrum was adjusted according to the detector response characteristics. X-ray excited photoluminescence spectra were measured at room temperature using an X-ray tube with U_a = 40 keV and I_a = 1 mA. A monochromator with 2 nm spectral resolution and an FEU-100 photomultiplier tube (170–830 nm) operating in single-photon counting mode were used for detection. X-ray excited luminescence decay kinetics were recorded within a 200 ns time gate, with ~1 ns X-ray pulses at a repetition frequency of 100 kHz. The integrated and time-resolved X-ray excited luminescence spectra were measured. The integrated luminescence spectrum was recorded over a 10 μs time window immediately after the X-ray excitation pulse. The slow component was measured using a 5 μs time window, with a delay of 750 ns after the X-ray excitation pulse. Persistent luminescence kinetics were recorded following X-ray exposure times of 5 and 15 min. In $RbCaF_3$:1 %Pr^{3+}, persistent luminescence intensity was scanned at 1-min intervals for 60 min. Thermoluminescence (TL) glow curves were measured by Lexsyg research – Fully Automated TL/OSL Reader (Freiberg Instruments GmbH). As the irradiation source X-Ray tube (VF-50 J/S RTG) with a copper body and tungsten as a target material by Varian (40 kV, 1 mA) was used. The TL glow curves were collected with an R13456 photomultiplier tube from Hamamatsu Photonics for the whole detection range with a neutral grey filter (NE20A-B - Ø25 mm Absorptive Neutral Density Filter). Before measurements, all samples were preheated to 350 °C. The TL parameters of $RbCaF_3$:Pr^{3+} were estimated by deconvoluting glow curve into discrete components using the GlowFIT software [27], based on a first-order kinetic model. The decay kinetics of persistent luminescence of $RbCaF_3$ samples with different activator concentrations were measured under identical conditions after 15 min of X-ray irradiation at room temperature. Due to the high luminescence intensity, a neutral grey filter (NE20A-B - Ø25 mm Absorptive Neutral Density Filter) was used during the measurements. All modules were operated using the LexStudio 2 software, which is dedicated to the operation of the TL/OSL Reader and supplied by the manufacturer.

2. Results and discussion

2.1. Crystal structure

Fig. 1a shows the XRPD patterns of undoped $RbCaF_3$ and $RbCaF_3$:1 % Pr^{3+}. All the patterns are single-phase and match well with the standard card for $RbCaF_3$, confirming a cubic structure (S.G. *Pm3m*). We assumed that due to the similar ionic radii of Ca^{2+} (1.00 Å, CN = 6) and Pr^{3+} (0.99 Å, CN = 6), Pr^{3+} ions occupy the Ca^{2+} position [28]. Since the ionic radii of praseodymium and calcium are very similar, no significant changes in the crystal lattice parameters were observed (Fig. 1S). Typically, during solid-phase synthesis and annealing, large, shapeless agglomerates form, as observed in the SEM images of $RbCaF_3$; the crystallite size is several tens of microns (Fig. 1b).

2.2. Luminescence properties using synchrotron radiation

Fig. 2a shows the luminescence excitation spectra recorded at 8 K and 250 K while monitoring at 480.5 nm. The excitation range from 160 to 225 nm is attributed to the interconfigurational transition from the ground level to the levels of the 4f5d electronic configuration of Pr^{3+}. This region can be divided into five components, indicating a low symmetry position for the praseodymium ion [29]. Both excitation spectra display bands corresponding to host lattice excitation in the 100–135 nm region [30]. The luminescence spectrum of $RbCaF_3$:1 % Pr^{3+} under 200 nm synchrotron excitation at low temperatures (T = 8 K) is attributed to both intra-configurational $4f^2 \rightarrow 4f^2$ and inter-configurational $4f5d \rightarrow 4f^2$ transitions of Pr^{3+} [31] (Fig. 2b, blue line). This indicates the proximity of the $^1S_0$ level to the $4f^1 5\ d^1$ configuration levels. Transitions from the latter, primarily to the $^3H_4$ and $^3H_6$ levels, are observed in the 220–320 nm region [31]. The $^1S_0 \rightarrow {}^3H_4$ transition appears at 215 nm, while subsequent peaks at 237.8, 250.4, 272.2, 335.2, and 394.4 nm correspond to the transitions from $^1S_0$ to the $^3H_6$, $^3F_3$, $^1G_4$, $^1D_2$, and $^1I_6$ levels, respectively. Among these, the $^1S_0 \rightarrow {}^1I_6$ transition exhibits the highest intensity. Furthermore, two emission peaks of comparable intensity are observed at 480.7 and 603 nm, attributed to the $^3P_0 \rightarrow {}^3H_4$ and $^3P_0 \rightarrow {}^3H_6$ transitions, respectively. The intensity distribution of the $^1S_0$ transitions presents the characteristic signature of the desired quantum cutting, with weaker emission in the ultraviolet region and stronger emission in the visible range. Notably, above 200 K, the $^1S_0$ emission is markedly suppressed in favor of the more intense $4f^1 5\ d^1 \rightarrow 4f^2$ emission. This behavior is also observed in other matrices activated by praseodymium ions, such as $BaSO_4$, $LiLaP_4O_{12}$ and $LiPrP_4O_{12}$ [32–34].

2.3. X-ray luminescence

In the X-ray excited luminescence spectrum of Pr^{3+}-doped $RbCaF_3$ (Fig. 3, curve 1), bands of 252 and 276 nm are observed, attributed to 5d-4f transitions of Pr^{3+} ions. Notably, the $^1S_0 \rightarrow {}^3P_J$ transition band at ~400 nm is absent from the X-ray excited luminescence spectrum compared to optical excitation at 8 K (Fig. 2b), confirming the $^1S_0$ level is slightly higher than the 5d levels. A similar $^1S_0$ location is observed in

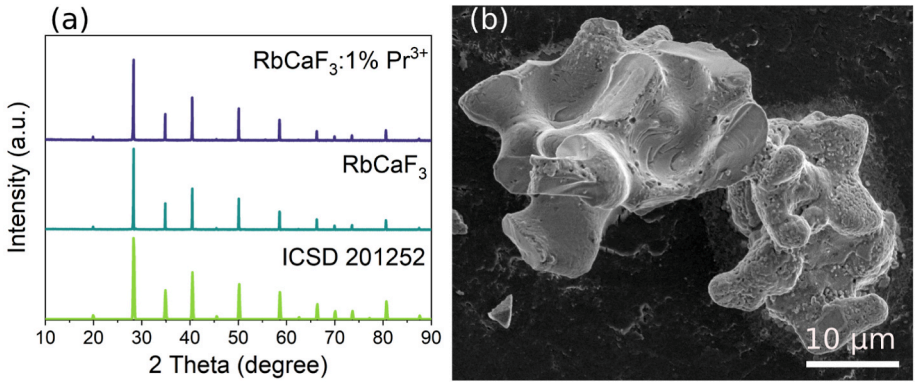

Fig. 1. (a) XRPD patterns of undoped $RbCaF_3$ and $RbCaF_3$:1 %Pr^{3+}, along with the standard card. (b) SEM image of $RbCaF_3$:1 %Pr^{3+} crystallites.

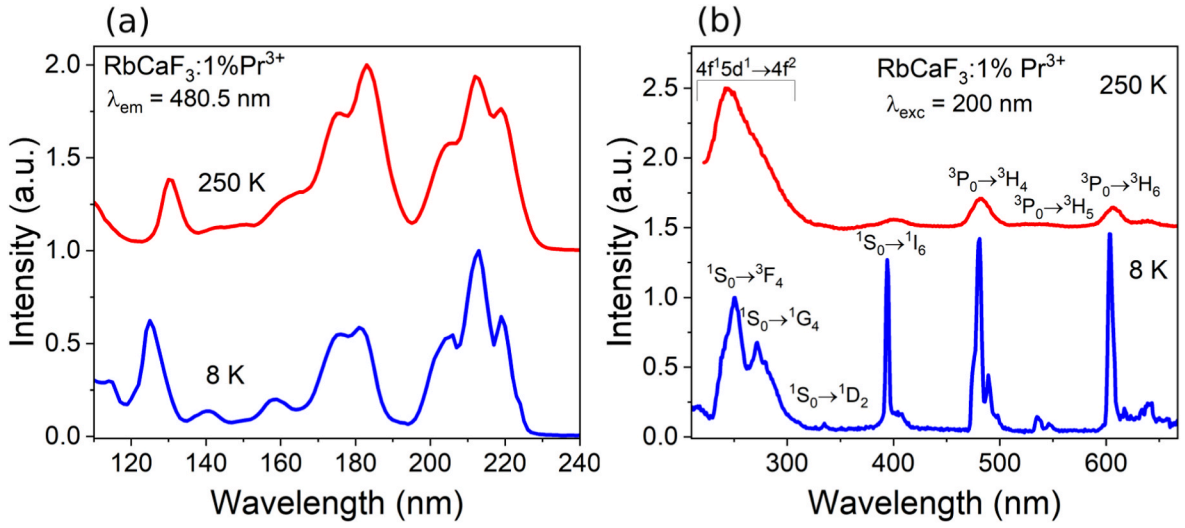

Fig. 2. (a) Excitation spectra of $RbCaF_3$:1 %Pr^{3+} recorded at 8 and 250 K using synchrotron radiation, monitoring 480.5 nm emission ($^3P_0 \rightarrow {}^3H_4$). (b) Emission spectra of $RbCaF_3$:1 %Pr^{3+} recorded at 8 and 230 K under 200 nm excitation using synchrotron radiation.

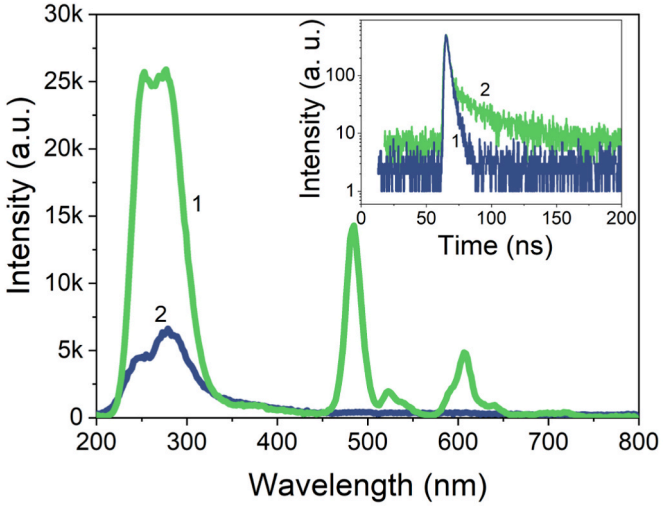

Fig. 3. Room temperature X-ray excited luminescence spectra of $RbCaF_3$:1 % Pr^{3+} (curve 1) and $RbCaF_3$ (curve 2). Inset: X-ray excited luminescence decay kinetics for the band with $\lambda_{max} = 260$ nm.

the $LiBaF_3$:Pr^{3+} [35] and $LiNaY_2F_8$:Pr^{3+} [36]. Other bands at 483, 523, and 607 nm correspond to $^3P_0 \rightarrow {}^3H_J$ transitions, which occur when the $^1I_6$, ^3P_J states are populated (see Fig. 3, curve 1) [33,35–37]. This population can arise from nonradiative transitions from the 5d levels to $^1I_6$, ^3P_J, or via nonradiative energy transfer from excitons to Pr^{3+} centers [35]. In the latter case, some electron-hole pairs generated during X-ray photon absorption relax to form excitons with sufficient energy to non-radiatively excite the $^1I_6$, ^3P_J levels, followed by a radiative $^3P_J \rightarrow {}^3H_J$ transition that produces the 483 nm emission band [36].

In the 200–400 nm range, the excited X-ray luminescence spectrum of undoped $RbCaF_3$ exhibits peaks at 245 nm and 280 nm (Fig. 3, curve 2). The 280 nm band demonstrates a short decay time of ~2.5 ns (Fig. 3 inset, curve 1), indicating the core-valence luminescence from the $RbCaF_3$ host [38]. For Pr^{3+}-doped $RbCaF_3$, the spectrum displays bands at 252 and 276 nm, attributed to 5d-4f luminescence of Pr^{3+} ions, which overlap the spectral range of the core-valence luminescence of the matrix. This is supported by the kinetic characteristics of the 260 nm band (Fig. 3 inset, curve 2), which shows two decay components: $\tau_1 = 2.5$ ns (core-valence luminescence) and $\tau_2 = 22$ ns, typical of 5d-4f luminescence of Pr^{3+}.

2.4. Persistent luminescence

A distinctive feature of $RbCaF_3$:1 %Pr^{3+} is its strong persistent luminescence, which lasts for a prolonged period after the X-ray excitation source is removed. The persistent luminescence spectra, recorded

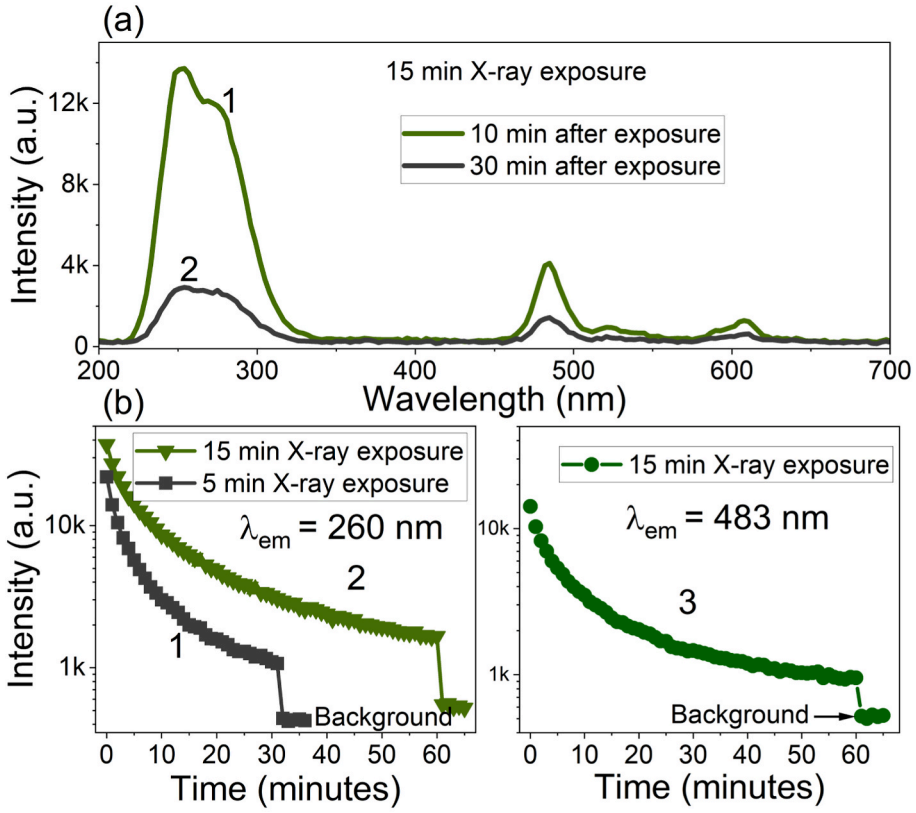

Fig. 4. (a) Persistent luminescence spectra of $RbCaF_3$:1 $\%Pr^{3+}$ recorded 10 min (curve 1) and 30 min (curve 2) after X-ray irradiation. (b) Persistent luminescence decay kinetics of $RbCaF_3$:1 $\%Pr^{3+}$: curves recorded following X-ray exposure times of 5 min (curve 1) and 15 min (curve 2) for λ_{em} = 260 nm, and a curve recorded after 15 min (curve 3) of X-ray exposure for λ_{em} = 483 nm, all at room temperature.

10 and 30 min after the cessation of X-ray excitation, are presented in Fig. 4a. This phenomenon may be attributed to the presence of traps in $RbCaF_3$:1 $\%Pr^{3+}$ that capture electrons [17,39,40]. Upon thermal stimulation, these trapped electrons are released and subsequently excite the luminescence of Pr^{3+} ions. As noted in Ref. [17], the duration of persistent luminescence depends on the number of trapped electrons – the more captured, the longer the emission persists. The X-ray luminescence spectrum under continuous excitation closely matches the persistent luminescence spectrum, both showing dominant 5d-4f bands at 252 nm and 276 nm. This suggests that the released electrons possess enough energy to excite the 5d-4f luminescence transitions of Pr^{3+} ions. Fig. 4b presents the persistent luminescence kinetics for the emission bands of 260 nm and 483 nm following different X-ray irradiation durations. The non-single-exponential decay suggests the presence of traps with different depths [17]. Moreover, Fig. 4b (curves 1 and 2) shows that longer X-ray irradiation of $RbCaF_3$:1 $\%Pr^{3+}$ leads to a slowdown in the persistent luminescence kinetics of the 260 nm band. This supports the idea that prolonged irradiation results in a higher number of trapped electrons, thus extending the persistent luminescence [17]. Curves 2 and 3 (Fig. 4b) exhibit similar decay patterns, allowing the evaluation of ultraviolet emission intensity (λ_{em} = 260 nm) through the measurement of visible emission intensity (λ_{em} = 483 nm) [40].

To compare the persistence of luminescence as a function of activator concentration, persistent luminescence decay curves in the visible region were measured after 15 min of irradiation using a grey filter Fig. 5. All measurements were conducted under identical conditions. As shown, the sample with a 1 % activator concentration exhibited the highest luminescence intensity Fig. 5. The persistent luminescence decay curves are well described by a double-exponential model, and the corresponding constants are presented in Table 1. As the activator concentration increases, a decrease in luminescence lifetimes is observed, which can be attributed to concentration quenching [5,40,41].

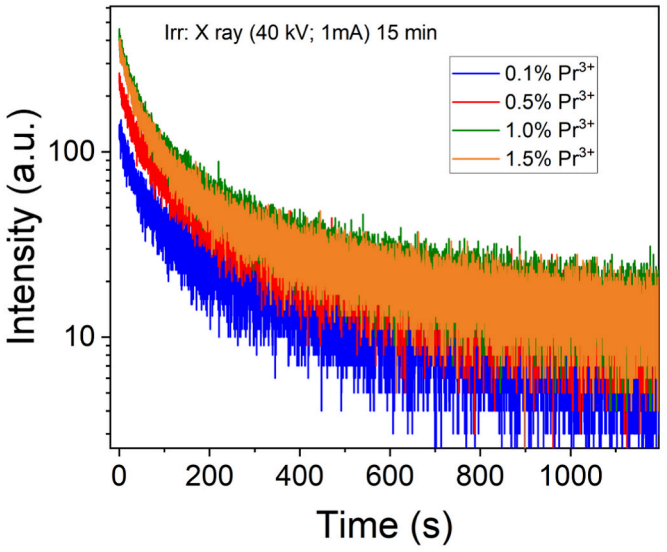

Fig. 5. Persistent luminescence decay kinetics of $RbCaF_3$ doped with 0.1–1.5 % Pr^{3+}, measured after 15 min of X-ray irradiation at room temperature using a neutral grey filter.

2.5. *Thermoluminescence spectrum*

Thermoluminescence (TL) analysis is a powerful method to determine the traps presence, their depths and redistribution by gradually heating preirradiated material and monitoring light emission as trapped charge carriers are released. To demonstrate that $RbCaF_3$:1 $\%Pr^{3+}$ contains traps at different energy levels, the TL glow curve was recorded

Table 1
The persistent luminescence decay time of $RbCaF_3:Pr^{3+}$ after irradiation for 15 min with X-rays at room temperature using the grey filter.

Concentration Pr^{3+}	τ_1 (s)	τ_2 (s)
0.1	38 ± 0.4	308 ± 4.2
0.5	39 ± 0.3	285 ± 2.9
1.0	36 ± 0.2	254 ± 2.0
1.5	35 ± 0.2	248 ± 2.0

after excitation with X-rays for 15 min at room temperature (Fig. 6). The shape of the TL glow curve for $RbCaF_3$:1 $\%Pr^{3+}$ is very similar to those observed in the thermoluminescence spectra of other fluoroperovskites [42,43]. Using the GlowFIT program, the TL glow curve was deconvoluted to estimate trap depths (Fig. S1) [27]. The TL peak maxima (T_M), activation energy (E), and corresponding frequency factors (s) are listed in Table 2. The figure of merit (FOM) for the curve fitting was 1.41 %, indicating a good fit. Analysis of the deconvolution data from Table 2 shows that, for some bands with maxima at higher temperatures, the activation energies are lower compared to those of bands with maxima at lower temperatures. This behaviour can be attributed to the frequency factor or the attempt-to-escape factor, which plays an important role in the de-trapping process [44–46]. The relationship between the frequency factor, the activation energy and temperature is described by the following equation (1) [44–46]:

$$\frac{\beta E}{kT_m^2} = s^* \exp\left\{-\frac{E}{kT_m}\right\}$$

where k is the Boltzmann constant (8.617×10^{-5} ev/K), and β is the heating rate (in K/s). A trap with a high frequency factor will require less energy (lower temperature) to carry the charge. Therefore, a trap with an energy of 1.1 eV is released at a lower temperature than traps with an energy of 0.5 eV. This dependence has also been observed in other compounds. Further studies are required to determine the exact nature of the traps in $RbCaF_3:Pr^{3+}$ and their influence on the observed persistent luminescence, which will be discussed in a future study.

2.6. Time-resolved X-ray luminescence

When X-rays are absorbed, part of the absorbed energy causes core-valence luminescence, part of the relaxed electron-hole pairs directly excites the 5d-4f luminescence of Pr^{3+}, and part of the relaxed electrons is captured by traps. As these trapped electrons are gradually released, they recombine with holes, exciting Pr^{3+} and leading to 5d → ^3H_J, ^3F_J emission, contributing to UVC persistent luminescence. Time-resolved X-ray luminescence measurements allowed the separation of the core-valence luminescence of the $RbCaF_3$ host and the 5d-4f luminescence of Pr^{3+} from the persistent luminescence. Fig. 7 presents the time-resolved X-ray luminescence spectra of $RbCaF_3:Pr^{3+}$ with a time delay of 750 ns?

Curve 1 (Fig. 7) represents the integral component, including core-valence luminescence and 5d-4f luminescence of Pr^{3+} ions, excited by both relaxed electron-hole pairs and trapped electrons. This aligns with the decay kinetics of the 260 nm band (Fig. 3, inset, curve 2), showing contributions from core-valence (2.5 ns) and 5d-4f luminescence of Pr^{3+} ion (22 ns). Curve 2 (Fig. 7) represents the slow component, which contains only 5d-4f luminescence excited by trapped electrons, without contributions from core-valence or directly excited 5d-4f luminescence of Pr^{3+} ions. As shown in Fig. 7, core-valence and directly excited 5d-4f luminescence of Pr^{3+} ions contribute only ~10 %, while ~90 % of the electron-hole pairs generated by X-ray absorption are captured by traps.

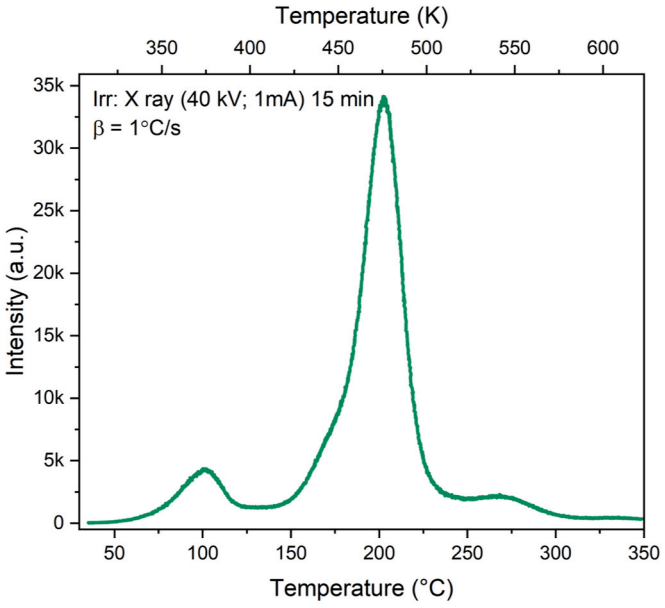

Fig. 6. TL glow curve of $RbCaF_3$:1 $\%Pr^{3+}$ after X-ray irradiation (40 kV, 1 mA) for 15 min at room temperature, heating rate of 1 °C/s.

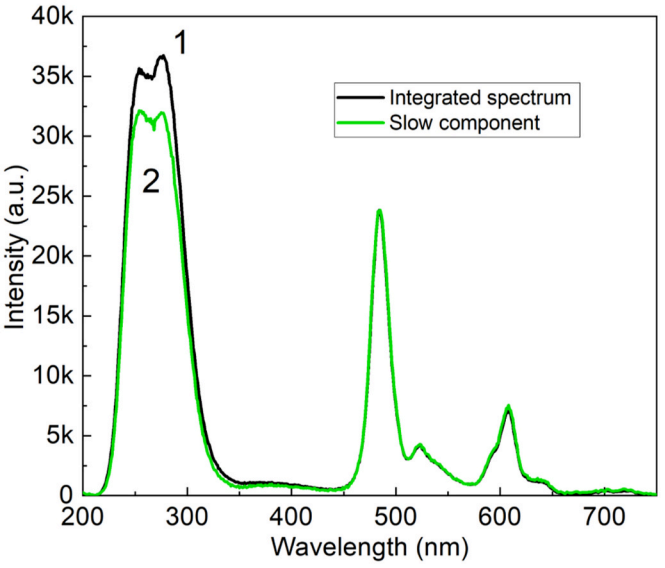

Fig. 7. Time-resolved X-ray excited luminescence spectra of $RbCaF_3:Pr^{3+}$ at room temperature: integrated spectrum (curve 1) and slow component (curve 2). The slow component was measured 750 ns after the excitation pulse within a time window of 5 μs time window. The spectra are normalized to the 483 nm band.

Table 2
Temperature of the maximum peak TL (T_M), activation energy (E) and frequency factor (s) obtained by fitting TL glow curves of $RbCaF_3$:1 $\%Pr^{3+}$ after X-ray irradiation (40 kV, 1 mA, 15 min) at a heating rate of 1 °C/s.

	1	2	3	4	5	6	7	8
T_M (K)	373	393	444	474	482	490	537	602
E (eV)	1.1	0.5	1.6	2.0	1.8	1.2	0.9	1.0
s (s^{-1})	10^{14}	10^6	10^{18}	10^{21}	10^{19}	10^{11}	10^8	10^7

Therefore, energy storage in traps is highly efficient, with slow energy release resulting in persistent luminescence, an important factor in radiotherapy [5,47,48]. To assess the novelty and practical significance of the obtained phosphor, Table 3 compares the luminescence persistence properties of $RbCaF_3:Pr^{3+}$ with those of other known persistent phosphors.

2.7. Possible X-ray–induced persistent luminescence mechanism

To understand the nature of persistent luminescence, it is necessary to consider the types of defects that can form in the $RbCaF_3$ matrix activated with Pr^{3+} ions. Doping the $RbCaF_3$ lattice with Pr^{3+} ions induces the formation of point defects to maintain local charge neutrality. Owing to the close similarity in ionic radii, Pr^{3+} ions are most likely to substitute for Ca^{2+} ions. In the absence of an intentional co-dopant for charge compensation, this substitution necessitates the creation of calcium vacancies (V_{Ca}) to balance the excess of positive charge, as represented by the following defect reaction [40,49]:

$$3Ca^{2+} \rightarrow 2Pr^{3+} + V_{Ca} \quad (1)$$

Additional charge compensation may occur by incorporating fluoride ions into interstitial lattice sites. Furthermore, the formation of rubidium vacancies (V_{Rb}) and the formation of local clusters $V_{Rb}PrF_3$-defects cannot be excluded. Although less probable due to the significant ionic size mismatch, exceeding 35 %—Pr^{3+} ions may also occupy Rb^{+} sites. This substitution would similarly require the generation of compensating defects described above.

The presence of multiple possible charge compensation mechanisms gives rise to persistent luminescence and manifests in the emission spectra as significant band broadening [40,49].In the case of band-to-band excitation of the $RbCaF_3$ matrix, electrons and holes formed in the conduction and valence bands, respectively, are captured by the aforementioned traps (Fig. 8). Due to thermal activation, the trapped carriers are released and subsequently recombine with Pr^{3+} ions according to the following scheme:

$$Pr^{3+} + h = Pr^{4+} \quad (2)$$

$$Pr^{4+} + e = \left(Pr^{3+}\right)^{*} = Pr^{3+} + hv. \quad (3)$$

As a result of this recombination, praseodymium in an excited state $(Pr^{3+})^*$ is formed. The decay of this excited state involves interconfigurational radiative 5d-^3H_J transitions and non-radiative transitions to the ^3P_J states. The decay of the ^3P_J states is accompanied by an intraconfigurational luminescence characteristic of praseodymium ions (see Fig. 8).

3. Conclusions

In summary, undoped $RbCaF_3$ and $RbCaF_3:Pr^{3+}$ crystallites were successfully synthesized using the solid-state method. X-ray-excited luminescence in the 200–400 nm range for undoped $RbCaF_3$ exhibits a decay constant of 2.5 ns, which can be attributed to the core-valence luminescence of the host material. In the X-ray luminescence spectrum of $RbCaF_3$:1 $\%Pr^{3+}$, the intense band at 260 nm can be described as a superposition of the 5d-4f luminescence of Pr^{3+} ions and the core-valence luminescence of the host material. An intense, long-persisting persistent luminescence (lasting more than 1 h) was observed in the $RbCaF_3$:1 $\%Pr^{3+}$ sample after irradiation with an X-ray source for 15 min. The persistent luminescence mechanism may be attributed to traps that capture electrons. The energy of electrons released from these traps is sufficient to excite the 5d-4f luminescence of Pr^{3+} ions. Increasing the X-ray exposure time to $RbCaF_3$:1 $\%Pr^{3+}$ leads to enhanced persistent luminescence kinetics. Detailed investigations using synchrotron radiation revealed simultaneous intra-configurational $4f^2 \rightarrow 4f^2$ and interconfigurational $4f5d \rightarrow 4f^2$ radiative transitions upon excitation of the 4f5d state in $RbCaF_3:Pr^{3+}$ crystallites. Due to its intense and, persistent luminescence following X-ray irradiation, $RbCaF_3$:1 $\%Pr^{3+}$ could be a promising material for medical applications, such as phototherapy for cancer treatment.

Table 3
A comprehensive overview of persistent UVC phosphors.

	Emission Centre	Maximum of Persistent Luminescence (nm)	Traps (eV)	Reference
$RbCaF_3$	Pr^{3+}	252, 276	0.5–2.0	This work
$Sr_2MgSi_2O_7$	Pr^{3+}	243	0.68–0.95	[41]
YPO_4	Bi^{3+}	240	0.44–0.97	[19]
Li_2CaGeO_4	Pr^{3+}	252	0.77–1.06	[21]
Cs_2NaYF_6	Pr^{3+}	250	0.69–1.02	[20]

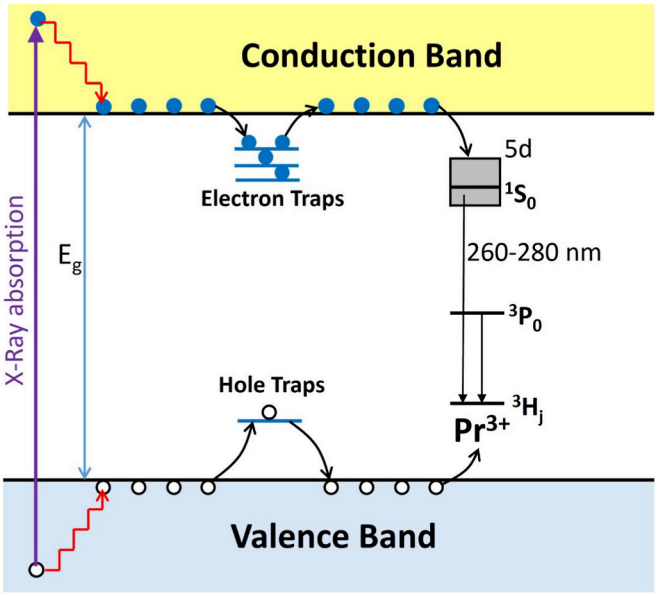

Fig. 8. Schematic representation of the persistent luminescence mechanism in the $RbCaF_3:Pr^{3+}$.

CRediT authorship contribution statement

Nadiia Rebrova: Writing – original draft, Investigation, Data curation. **Andriy Pushak:** Writing – original draft, Investigation, Data curation. **Alexander Grippa:** Writing – original draft, Investigation, Data curation. **Vitalii Boiko:** Data curation, Investigation. **Patrycja Zdeb-Stańczykowska:** Investigation, Data curation. **Anatoliy Voloshinovskii:** Writing – original draft, Investigation, Data curation. **Przemysław J. Dereń:** Writing – original draft, Supervision, Project administration, Methodology, Funding acquisition, Conceptualization.

Declaration of competing interest

The authors declare that they have no known competing financial interests or personal relationships that could have appeared to influence the work reported in this paper.

Acknowledgment

This work was supported by grant no. 2021/41/B/ST5/03792, for which we are very grateful. The investigation using synchrotron radiation at the P66 SUPERLUMI station at DESY, Hamburg, Germany was a performed within the framework of I-20240194 EC project. One of the authors, A. Grippa (Oleksandr Gryppa), thanks the Polish Academy of Sciences for their support through the PAN-NANU (PAS-NASU) program

for scientists cooperating with INTiBS PAN.

Appendix A. Supplementary data

Supplementary data to this article can be found online at https://doi.org/10.1016/j.jlumin.2025.121333.

Data availability

Data will be made available on request.

References

[1] R.L. Siegel, A.N. Giaquinto, A. Jemal, Cancer statistics, CA Cancer J. Clin. 74 (2024) 12–49, https://doi.org/10.3322/caac.21820, 2024.

[2] Z.W. Yu, M. Zheng, H.Y. Fan, X.H. Liang, Y.L. Tang, Ultraviolet (UV) radiation: a double-edged sword in cancer development and therapy, Molecular Biomedicine 5 (2024), https://doi.org/10.1186/s43556-024-00209-8.

[3] M. Momiyama, A. Suetsugu, H. Kimura, H. Kishimoto, R. Aki, A. Yamada, H. Sakurada, T. Chishima, M. Bouvet, I. Endo, R.M. Hoffman, Imaging the efficacy of UVC irradiation on superficial brain tumors and metastasis in live mice at the subcellular level, J. Cell. Biochem. 114 (2013) 428–434, https://doi.org/10.1002/jcb.24381.

[4] L. Finlayson, I.R.M. Barnard, L. McMillan, S.H. Ibbotson, C.T.A. Brown, E. Eadie, K. Wood, Depth penetration of light into skin as a function of wavelength from 200 to 1000 nm, Photochem. Photobiol. 98 (2022) 974–981, https://doi.org/10.1111/php.13550.

[5] Y. Zhang, S. Yan, F. Xiao, X. Shan, X. Lv, W. Wang, Y. Liang, Long-persistent far-UVC light emission in Pr3+-doped Sr2P2O7 phosphor for microbial sterilization, Inorg. Chem. Front. 10 (2023) 5958–5968, https://doi.org/10.1039/D3QI01253K.

[6] S. Espinoza, M. Müller, H. Jenneboer, L. Peulen, T. Bradley, M. Purschke, M. Haase, R. Rahmanzadeh, T. Jüstel, Characterization of micro- and nanoscale LuPO4:Pr3+, Nd3+ with strong UV-C emission to reduce X-ray doses in radiation therapy, Part. Part. Syst. Char. 36 (2019), https://doi.org/10.1002/ppsc.201900280.

[7] M. Müller, S. Espinoza, T. Jüstel, K.D. Held, R.R. Anderson, M. Purschke, UVC-emitting LuPO4:Pr3+ nanoparticles decrease radiation resistance of hypoxic cancer cells, Radiat. Res. 193 (2019) 82–87, https://doi.org/10.1667/RR15491.1.

[8] W. Yen, M. Weber, Inorganic phosphors: compositions, preparation and optical properties. https://doi.org/10.1201/9780203506325, 2004.

[9] T. Matsuzawa, Y. Aoki, N. Takeuchi, Y. Murayama, A new long phosphorescent phosphor with high brightness, SrAl2 O 4 : Eu2 + , Dy3 +, J. Electrochem. Soc. 143 (1996) 2670, https://doi.org/10.1149/1.1837067.

[10] T. Aitasalo, P. Dereń, J. Hölsä, H. Jungner, J.-C. Krupa, M. Lastusaari, J. Legendziewicz, J. Niittykoski, W. Stręk, Persistent luminescence phenomena in materials doped with rare earth ions, J. Solid State Chem. 171 (2003) 114–122, https://doi.org/10.1016/S0022-4596(02)00194-9.

[11] S. Yang, W. Guo, Z. Tang, Z. Zhang, H. Guo, Y. Lao, B. Qu, L. Xiao, J. Shi, Z. Chen, Long-persistent luminescence from double self-defect states in undoped Cs3In2Cl9 nanocrystals for bioimaging and display technologies, ACS Appl. Nano Mater. 5 (2022) 9469–9477, https://doi.org/10.1021/acsanm.2c01738.

[12] R. Yang, D. Yang, M. Wang, F. Zhang, X. Ji, M. Zhang, M. Jia, X. Chen, D. Wu, X. J. Li, Y. Zhang, Z. Shi, C. Shan, High-Efficiency and stable long-persistent luminescence from undoped cesium cadmium chlorine crystals induced by intrinsic point defects, Adv. Sci. 10 (2023) 2207331, https://doi.org/10.1002/advs.202207331.

[13] I. Norrbo, J.M. Carvalho, P. Laukkanen, J. Mäkelä, F. Mamedov, M. Peurla, H. Helminen, S. Pihlasalo, H. Härmä, J. Sinkkonen, M. Lastusaari, Lanthanide and heavy metal free long white persistent luminescence from Ti doped Li–hackmanite: a versatile, low-cost material, Adv. Funct. Mater. 27 (2017) 1606547, https://doi.org/10.1002/adfm.201606547.

[14] L. Li, T. Li, Y. Hu, C. Cai, Y. Li, X. Zhang, B. Liang, Y. Yang, J. Qiu, Mechanism of the trivalent lanthanides' persistent luminescence in wide bandgap materials, Light Sci. Appl. 11 (2022) 51, https://doi.org/10.1038/s41377-022-00736-5.

[15] L. Liang, J. Chen, K. Shao, X. Qin, Z. Pan, X. Liu, Controlling persistent luminescence in nanocrystalline phosphors, Nat. Mater. 22 (2023) 289–304, https://doi.org/10.1038/s41563-022-01468-y.

[16] T. Lyu, P. Dorenbos, Bi3+ acting both as an electron and as a hole trap in La-, Y-, and LuPO4, J Mater Chem C Mater 6 (2018) 6240–6249, https://doi.org/10.1039/C8TC01020J.

[17] C. Li, X. Cai, Y. Qiang, X. Shi, Y. Jiang, Y. Chen, F. Lai, B. Wang, Y. Leng, W. You, Mechanism analysis on manipulation of long afterglow luminescence properties of Y3Al5-xGaxO12:Ce3+, Cr3+ phosphors, J. Lumin. 270 (2024) 120537, https://doi.org/10.1016/j.jlumin.2024.120537.

[18] J. Hölsä, Persistent luminescence beats the afterglow: 400 Years of persistent luminescence, Electrochem. Soc. Interface 18 (2009) 42, https://doi.org/10.1149/2.F06094IF.

[19] Q. Liu, Z.-Y. Feng, H. Li, Q. Zhao, N. Shirahata, Y. Kuroiwa, C. Moriyoshi, C.-K. Duan, H.-T. Sun, Non-Rare-Earth UVC persistent phosphors enabled by bismuth doping, Adv. Opt. Mater. 9 (2021) 2002065, https://doi.org/10.1002/adom.202002065.

[20] Y.-M. Yang, Z.-Y. Li, J.-Y. Zhang, Y. Lu, S.-Q. Guo, Q. Zhao, X. Wang, Z.-J. Yong, H. Li, J.-P. Ma, Y. Kuroiwa, C. Moriyoshi, L.-L. Hu, L.-Y. Zhang, L.-R. Zheng, H.-T. Sun, X-ray-activated long persistent phosphors featuring strong UVC afterglow emissions, Light Sci. Appl. 7 (2018) 88, https://doi.org/10.1038/s41377-018-0089-7.

[21] X. Zhou, J. Qiao, Y. Zhao, K. Han, Z. Xia, Multi-responsive deep-ultraviolet emission in praseodymium-doped phosphors for microbial sterilization, Sci. China Mater. 65 (2022) 1103–1111, https://doi.org/10.1007/s40843-021-1790-1.

[22] X. Wang, Y. Chen, F. Liu, Z. Pan, Solar-blind ultraviolet-C persistent luminescence phosphors, Nat. Commun. 11 (2020) 2040, https://doi.org/10.1038/s41467-020-16015-z.

[23] Y. Zhang, X. Shan, X. Lv, D. Chen, S. Miao, W. Wang, Y. Liang, Multimodal luminescence in Pr3+ single-doped Li2CaSiO4 phosphor for optical information storage and anti-counterfeiting applications, Chem. Eng. J. 474 (2023) 145886, https://doi.org/10.1016/j.cej.2023.145886.

[24] Y. Liu, S. Yan, T. Wang, Q. He, X. Zhu, C. Wang, D. Liu, T. Wang, X. Xu, X. Yu, Achieving color-tunable long persistent luminescence in Cs2CdCl4 ruddlesden-popper phase perovskites, Angew. Chem. Int. Ed. 62 (2023) e202308420, https://doi.org/10.1002/anie.202308420.

[25] G.V.M. Williams, C. Dotzler, A. Edgar, S. Raymond, Optically rewritable Bragg gratings in Mn2+ doped RbCdF3, J. Mater. Sci. Mater. Electron. 20 (2009) 268–271, https://doi.org/10.1007/s10854-008-9572-x.

[26] N. Rebrova, A. Grippa, P. Zdeb, P.J. Dereń, Blue to UV upconversion properties of Pr3+ doped ACaF3 (A = K, Rb, Cs) phosphors, Scr. Mater. 255 (2025) 116395, https://doi.org/10.1016/j.scriptamat.2024.116395.

[27] M. Puchalska, P. Bilski, GlowFit—a new tool for thermoluminescence glow-curve deconvolution, Radiat. Meas. 41 (2006) 659–664, https://doi.org/10.1016/j.radmeas.2006.03.008.

[28] R.D. Shannon, Revised effective ionic radii and systematic studies of interatomic distances in halides and chalcogenides, Acta Crystallogr. A 32 (1976) 751–767, https://doi.org/10.1107/S0567739476001551.

[29] E. van der Kolk, P. Dorenbos, C.W.E. van Eijk, Vacuum ultraviolet excitation of 1S0 and 3P0 emission of Pr3+ in Sr0.7La0.3Al11.7Mg0.3O19 and SrB4O7, J. Phys. Condens. Matter 13 (2001) 5471, https://doi.org/10.1088/0953-8984/13/23/306.

[30] M.J. Knitel, P. Dorenbos, C.W.E. van Eijk, B. Plasteig, B. Viana, A. Kahn-Harari, D. Vivien, Photoluminescence, and scintillation/thermoluminescence yields of several Ce3+ and Eu2+ activated borates, Nucl. Instrum. Methods Phys. Res. 443 (2000) 364–374, https://doi.org/10.1016/S0168-9002(99)01154-7.

[31] A.M. Srivastava, A.A. Setlur, H.A. Comanzo, W.W. Beers, U. Happek, P. Schmidt, The influence of the Pr3+ 4f15d1 configuration on the 1S0 emission efficiency and lifetime in LaPO4, Opt. Mater. 33 (2011) 292–298, https://doi.org/10.1016/j.optmat.2010.08.026.

[32] A.P. Vink, P. Dorenbos, C.W.E. van Eijk, Thermal population of the (formula presented) state in (formula presented), Phys. Rev. B Condens. Matter Mater Phys 66 (2002) 1–6, https://doi.org/10.1103/PhysRevB.66.075118.

[33] T. Shalapska, G. Stryganyuk, Y. Romanyshyn, D. Trots, P. Demchenko, A. Gektin, A. Voloshinovskii, P. Dorenbos, Photon cascade luminescence from Pr3+ ions in LiPrP4O12 polyphosphate, J. Phys. D Appl. Phys. 43 (2010) 405404, https://doi.org/10.1088/0022-3727/43/40/405404.

[34] A.M. Srivastava, A.A. Setlur, H.A. Comanzo, M.E. Hannah, P.A. Schmidt, U. Happek, Luminescence from the Pr3+ 4f15d1 and 1S0 states in LiLaP4O12, J. Lumin. 129 (2009) 126–129, https://doi.org/10.1016/j.jlumin.2008.08.008.

[35] P. Zdeb-Stańczykowska, A. Grippa, P.J. Dereń, A. Voloshinovskii, A. Pushak, Y. Smortsova, N. Rebrova, Luminescent properties of Pr3+-doped LiBaF3 crystallites, Inorg. Chem. 64 (2025) 1379–1388, https://doi.org/10.1021/acs.inorgchem.4c04443.

[36] P. Zdeb-Stańczykowska, N. Rebrova, Y. Zorenko, A. Voloshinovskii, A. Pushak, P. J. Dereń, Multifunctional Pr3+-doped LiNaY2F8 phosphor for visible-to-UVC and X-ray-to-UVC conversion, J. Alloys Compd. 1016 (2025) 178807, https://doi.org/10.1016/j.jallcom.2025.178807.

[37] A.M. Srivastava, M. Jennings, J. Collins, The interconfigurational (4f15d1→4f2) luminescence of Pr3+ in LuPO4, K3Lu(PO4)2 and LiLuSiO4, Opt. Mater. 34 (2012) 1347–1352, https://doi.org/10.1016/j.optmat.2012.02.016.

[38] A.N. Belsky, P. Chevallier, E.N. Mel'chakov, C. Pédrini, P.A. Rodnyi, A.N. Vasil'ev, Luminescence properties of the RbCaF3 crystal at X-ray excitation, Chem. Phys. Lett. 278 (1997) 369–372, https://doi.org/10.1016/S0009-2614(97)01035-X.

[39] J. Ueda, K. Aishima, S. Nishiura, S. Tanabe, Afterglow luminescence in Ce3+-doped Y3Sc2Ga3O12 ceramics, APEX 4 (2011) 042602, https://doi.org/10.1143/APEX.4.042602.

[40] J. Zhang, R. Liu, X. Fu, J. Yi, T. Lin, Z. Liu, N. Chen, H. Zhang, X-ray–induced multicolor long afterglow and photostimulated luminescence from Pr3+-doped Sr3(PO4)2, J. Am. Ceram. Soc. 108 (2025) e20204, https://doi.org/10.1111/jace.20204.

[41] A. Antuzevics, G. Doke, G. Krieke, P. Rodionovs, D. Nilova, J. Cirulis, A. Fedotovs, U. Rogulis, Shortwave ultraviolet persistent luminescence of Sr2MgSi2O7: Pr3+, Materials 16 (2023) https://doi.org/10.3390/ma16051776.

[42] C. Furetta, F. Santopietro, C. Sanipoli, G. Kitis, Thermoluminescent (TL) properties of the perovskite KMgF3 activated by Ce and Er impurities, Appl. Radiat. Isot. 55 (2001) 533–542, https://doi.org/10.1016/S0969-8043(01)00085-9.

[43] L. Pérez-Cruz, E. Cruz-Zaragoza, D. Díaz, J.M.H. Alcántara, E.C. García, I. Camarillo-García, H.M. Sánchez, Synthesis, optical and thermoluminescence properties of thulium-doped KMgF3 fluoroperovskite, Appl. Radiat. Isot. 177 (2021) 109913, https://doi.org/10.1016/j.apradiso.2021.109913.

[44] V. Boiko, Z. Dai, M. Chaika, K. Grzeszkiewicz, J. Li, W. Strek, D. Hreniak, Size-dependent persistent luminescence of YAGG:Cr3+ nanophosphors, Materials 15 (2022), https://doi.org/10.3390/ma15134407.

[45] M. Mashangva, N. Singh, Th, B. Singh, Estimation of Optimal Trapping Parameters Relevant to Persistent Luminescence, 2011.
[46] A.J.J. Bos, Theory of thermoluminescence, Radiat. Meas. 41 (2006), https://doi.org/10.1016/j.radmeas.2007.01.003.
[47] Y. Jiang, J. Huang, X. Zhen, Z. Zeng, J. Li, C. Xie, Q. Miao, J. Chen, P. Chen, K. Pu, A generic approach towards afterglow luminescent nanoparticles for ultrasensitive in vivo imaging, Nat. Commun. 10 (2019) 2064, https://doi.org/10.1038/s41467-019-10119-x.
[48] C. Chen, H. Gao, H. Ou, R.T.K. Kwok, Y. Tang, D. Zheng, D. Ding, Amplification of activated near-infrared afterglow luminescence by introducing twisted molecular geometry for understanding neutrophil-involved diseases, J. Am. Chem. Soc. 144 (2022) 3429–3441, https://doi.org/10.1021/jacs.1c11455.
[49] T.M. Demkiv, YaM. Chornodolskyy, T.M. Muzyka, S.Z. Malynych, R.Y. Serkiz, A. S. Pushak, A. Kotlov, R. V Gamernyk, Effect of Yb doping on the optical and photoelectric properties of CsPbCl3 single crystals, Opt. Mater. X 22 (2024) 100303, https://doi.org/10.1016/j.omx.2024.100303.